Fully relativistic description of magnetic Compton profiles with an application to UFe_2

D. Benea,[1] S. Mankovsky,[2] and H. Ebert[2]
[1]*Babes-Bolyai University, Kluj-Napoca, Romania*
[2]*Department Chemie und Biochemie, Universität München, Butenandtstrasse 5-13, D-81377 München, Germany*
(Received 15 November 2005; published 14 March 2006)

The magnetic Compton profile of UFe_2 has been calculated using the spin-polarized relativistic Korringa-Kohn-Rostoker band-structure method. For this purpose a corresponding fully relativistic scheme to determine the magnetic Compton profile has been developed. This approach accounts for magnetism as well as all relativistic effects on the same footing, as it is indispensable when dealing with the electronic structure of magnetic compounds containing heavy elements. Results obtained for the magnetic Compton profile of UFe_2 are found in good agreement with experimental data of Lawson*et al.* An analysis of the component-resolved contributions to the magnetic Compton profile shows that there is no strict one-to-one relation to the corresponding spin moments. In addition an appreciable site-site interference contribution is found.

DOI: 10.1103/PhysRevB.73.094411 PACS number(s): 75.25.+z, 71.15.Ap

I. INTRODUCTION

In recent years, the study of actinides and actinide compounds has attracted much interest because of the great variety of the magnetic behavior, such as Pauli paramagnetism, localized or itinerant magnetism, and heavy-fermion behavior. The complexity of the magnetic behavior is partially connected with the strength of the spin-orbit coupling, which is rather large compared with the crystal field energy. In particular, the spin-orbit-coupling-induced orbital magnetic moment can be appreciable if the strength of the coupling is comparable to the *f*-band width.

Although *f* electrons in actinides often show a localized behavior, there are also many compounds for which an itinerant description is more appropriate; i.e., the *f* states are strongly hybridized with the conduction band (*s*, *p*, and *d*) giving rise to unusual properties. One consequence of the delocalization is the formation of compounds with ordered magnetic moments, which are much smaller than those anticipated from localized *f* electrons.[1] This 5*f*-electron delocalization has been reported in particular for the UFe_2 compound.[2] UFe_2 is a ferromagnet with a Curie temperature of 160 K, which crystallizes in the cubic Laves phase and has low magnetic anisotropy. Neutron diffraction experiments[3–5] found a very small total moment in this system. The orbital and spin magnetic moments, which individually have a value of $\sim 0.23\mu_B$, almost completely cancel on the U sublattice. The magnetic circular x-ray dichroism (XMCD) investigations of the U *M* edge[6] using the sum rules confirmed the virtual cancellation of the spin and orbital moments of U.

From spin-polarized linear muffin-tin orbital (LMTO) band-structure calculations[7,2] a 5*f* orbital moment on the U site $\mu_{orb}=0.47\mu_B$ was found that is oriented antiparallel to the spin moment $\mu_{spin}=-0.58\mu_B$. Adding the small *s*, *p*, and *d* contributions, the total U moment is $-0.24\mu_B$ per atom with the sign indicating that it is antiparallel to the larger Fe moment $(0.77\mu_B)$.

Neutron experiments are sensitive to the total site magnetization, which for U in UFe_2 is very small. Magnetic dichroism experiments, on the other hand, are element specific. Unfortunately, the corresponding available XMCD data do not show a complete picture of the UFe_2 magnetism so far. For these reasons, magnetic Compton scattering experiments have been performed by Lawson *et al.*[8] in order to get information about the spin magnetization of this compound. The measured profile was fitted by free-atom magnetic Compton profiles for Fe 3*d*, U 5*f*, and a diffuse component, modeled as the sum of a U 6*d* free-atom profile and a free-electron parabola smeared with the experimental resolution function. Following this empirical procedure, they obtained spin moments for 5*f* U and 3*d* Fe in agreement with those deduced from neutron measurements.

The aim of the present work is to supply a sound theoretical basis for a detailed discussion of the magnetic Compton profile for compounds containing heavy elements and this way in particular for UFe_2. For this purpose an appropriate computational scheme has been developed that is based on the Korringa-Kohn-Rostoker (KKR) band-structure method. Our scheme can be seen as an extension of the previous work of Mijnarends and Bansil[9] and Gyorffy and Stocks.[10] These authors developed a scheme to calculate the momentum density in disordered alloys by making use of the KKR band-structure method combined with the coherent potential approximation (CPA) alloy theory. In contrast to these works we present a fully relativistic formulation that can be applied in particular to magnetic solids with many atoms per unit cell. In addition we make use of an integration in the complex energy plane that reduces the numerical effort in an appreciable way. A combination with the CPA alloy theory, not needed in the following for the ordered compound UFe_2, can be done in analogy to the work of Stocks and Gyorffy[10] who considered systems with one site per unit cell. This great flexibility of the KKR method used here stems from the use of the electronic Green's function to represent the electronic structure. All other previous theoretical investigations of Compton scattering aways ignored the influence of spin-orbit coupling and used conventional band-structure methods with the electronic structure represented by means of Bloch wave functions and associated energy eigenvalues.[11–13]

Our computational scheme together with the main features of the underlying electronic structure calculations will be presented in the next sections. The main part of this contribution is devoted to a presentation of our results for UFe_2 and a comparison with experiment.

II. THEORETICAL FRAMEWORK

A. Band-structure calculations

The electronic structure of the UFe_2 in the cubic Laves phase (lattice parameter a_{lat}=7.06 Å) was calculated self-consistently by means of the spin-polarized relativistic Korringa-Kohn-Rostoker (SPR-KKR) method in the atomic sphere approximation (ASA) mode.[14,15] The calculation scheme is based on the KKR Green's function formalism, which makes use of multiple-scattering theory. This means that the electronic structure is not represented by means of Bloch wave functions and eigenenergies but the electronic Green's function $G(\vec{r},\vec{r}',E)$. Within the multiple-scattering formalism $G(\vec{r},\vec{r}',E)$ is given for an ordered system with many atom sites per unit cell by

$$G(\vec{r},\vec{r}',E) = \sum_{\Lambda\Lambda'} Z^q_\Lambda(\vec{r},E)\tau^{nqn'q'}_{\Lambda\Lambda'}(E)Z^{q'\times}_{\Lambda'}(\vec{r}',E) - \sum_{\Lambda}[Z^q_\Lambda(\vec{r},E)J^{q\times}_\Lambda(\vec{r}',E)\Theta(r'-r) + J^q_\Lambda(\vec{r},E)Z^{q\times}_\Lambda(\vec{r}',E)\Theta(r-r')]\delta_{nn'}\delta_{qq'}. \quad (1)$$

Here $\vec{r}(\vec{r}')$ is assumed to be within the unit cell $n(n')$ and atomic site $q(q')$ and $\tau^{nqn'q'}_{\Lambda\Lambda'}(E)$ is the scattering path operator with the combined index $\Lambda=(\kappa,\mu)$ standing for the spin-orbit and magnetic quantum numbers κ and μ, respectively.[16] Finally, the four-component wave functions Z^q_Λ and J^q_Λ are the regular and irregular, respectively, solutions to the single-site Dirac equation for the atomic site q.

Details of the calculation method have been described in details elsewhere.[15,17] Exchange and correlation effects were treated within the framework of the local spin density approximation (LSDA) to spin density functional theory, using the parametrization of Vosko, Wilk, and Nusair.[18]

B. Magnetic Compton profile

Magnetic Compton scattering is a well-established technique for probing the spin-dependent momentum densities of magnetic solids.[11,19,20] If one considers an incident photon with wave vector $\vec{k}_0$ and a scattered photon with the wave vector $\vec{k}'$, the magnetic Compton cross section for a solid can be written within the impulse approximation as[13]

$$\left[\frac{d^2\sigma}{d\Omega dp_z}\right]_\uparrow - \left[\frac{d^2\sigma}{d\Omega dp_z}\right]_\downarrow \equiv \left[\frac{d^2\sigma}{d\Omega dp_z}\right]_\Delta = P_c r_0^2\left(\frac{k'^2}{k_0^2}\right)\Psi_2(\sigma)J_{mag}(p_z), \quad (2)$$

where P_c is the degree of circular polarization of the radiation, r_0 is the classical electron radius, and Ψ_2 is a geometrical factor, defined as

$$\Psi_2 = \pm\sigma[k_0\cos\alpha\cos\varphi - k'\cos(\alpha-\varphi)](\cos\varphi-1)\frac{\hbar c}{m_0c^2}. \quad (3)$$

In this formula, σ is the electron spin (±1), α is the angle between the incident photon ($\vec{k}_0$) and the magnetization direction ($\vec{M}$), and φ is the scattering angle. J_{mag} is the momentum distribution of the unpaired electrons projected along the scattering vector (p_z), also known as the magnetic Compton profile:

$$J_{mag}(p_z) = \int\int [n^\uparrow(\vec{p}) - n^\downarrow(\vec{p})]dp_x dp_y. \quad (4)$$

Here the electron momentum density for a given spin orientation is given by $n^{\uparrow(\downarrow)}(\vec{p})$.

The area under the magnetic Compton profile is equal to the spin moment per unit cell:

$$\int_{-\infty}^{+\infty} J_{mag}(p_z)dp_z = \mu_{spin}. \quad (5)$$

In order to calculate the magnetic Compton profile $J_{mag}(p_z)$ using the SPR-KKR band-structure method, one has to express the spin-projected momentum density $n^{m_s}(\vec{p})$ by means of the Green's function in momentum space:

$$n^{m_s}(\vec{p}) = -\frac{1}{\pi}\int_0^{E_F} \mathrm{Im}\, G_{m_s}(\vec{p},\vec{p},E)dE, \quad (6)$$

where m_s represents the spin character. $G_{m_s}(\vec{p},\vec{p}',E)$ can be expressed in terms of the real-space Green's function $G(\vec{r},\vec{r}',E)$ according to

$$G_{m_s m_s'}(\vec{p},\vec{p}',E) = \frac{1}{N\Omega}\int d^3r\int d^3r'\Phi^\times_{\vec{p}m_s}(\vec{r})\mathrm{Im} \times G^+(\vec{r},\vec{r}',E)\Phi_{\vec{p}'m_s'}(\vec{r}'). \quad (7)$$

Here Ω is the volume of the unit cell and $\Phi_{\vec{p}m_s}$ are the eigenfunctions of the momentum operator, which can be written as $\Phi_{\vec{p}m_s}=U_{\vec{p}m_s}e^{i\vec{p}\vec{r}}$, where $U_{\vec{p}m_s}$ is a four-component spinor satisfying the equation[16]

$$(c\vec{\alpha}\vec{p} + \beta mc^2)U_{\vec{p}m_s} = E_p U_{\vec{p}m_s}. \quad (8)$$

The expression for the eigenfunctions in momentum representation reads

$$\Phi_{\vec{p}m_s} = U_{\vec{p}m_s}e^{i\vec{p}\cdot\vec{r}} = \left(\frac{E_p+c^2}{2E_p+c^2}\right)^{1/2}\begin{pmatrix}\chi_{m_s}\\ \dfrac{c\vec{\sigma}\cdot\vec{p}}{E_p+c^2}\chi_{m_s}\end{pmatrix}e^{i\vec{p}\cdot\vec{r}}, \quad (9)$$

where

$$E_p = \frac{c^2}{2}\left(\sqrt{1+\frac{p^2}{c^2}}-1\right) \tag{10}$$

is the electron's total energy, χ_{m_s} are the Pauli spinors, and m_s is the spin quantum number. Using the expansion[16]

$$\chi_{m_s} e^{i\vec{p}\cdot\vec{r}} = 4\pi\sum_{\Lambda} i^l C_{\Lambda}^{m_s} Y_l^{\mu-m_s *}(\vec{p}) j_l(pr)\chi_{\Lambda} \tag{11}$$

and the properties of the operator $\vec{\sigma}\cdot\vec{p}$, these functions are rewritten as

$$\Phi_{\vec{p}m_s} = 4\pi\left(\frac{E_p+c^2}{2E_p+c^2}\right)^{1/2}\sum_{\Lambda} i^l C_{\Lambda}^{m_s} Y_l^{\mu-m_s *}(\vec{p}) \times\begin{pmatrix} j_l(pr)\chi_{\Lambda}(\hat{r}) \\ \dfrac{icS_k}{E_p+c^2} j_{\bar{l}}(pr)\chi_{-\Lambda}(\hat{r}) \end{pmatrix}, \tag{12}$$

where $C_{\Lambda}^{m_s}$ are the Clebsch-Gordan coefficients, $Y_l^{m_l}$ are the complex spherical harmonics, $\chi_{\Lambda}(\hat{r})$ are the spin-angular functions, and $j_l(pr)$ are the spherical Bessel functions.[16]

To deal with Eq. (7) one may write $\vec{r}=\vec{R}_n+\vec{r}_n$ where $\vec{R}_n$ is the origin of the nth cell and $\vec{r}_n$ is restricted to cell n. In addition, one may consider the real-space integration $\int d^3r$ as a summation over the cell integrals $\int d^3r = \Sigma_n \int d^3r_n$. Consequently, the expression for the Green's function reads

$$\begin{aligned} G_{m_s m_s'}(\vec{p},\vec{p}',E) &= \frac{1}{N\Omega}\sum_n \int d^3r_n \int d^3r' \Phi^{\times}_{\vec{p}m_s}(\vec{R}_n+\vec{r}_n) \\ &\quad\times \mathrm{Im}\, G^{+}(\vec{R}_n+\vec{r}_n,\vec{r}',E)\Phi_{\vec{p}'m_s'}(\vec{r}') \\ &= \frac{1}{N\Omega}\sum_n \int d^3r_n \int d^3r' U^{\times}_{\vec{p}m_s} e^{-i\vec{p}\cdot(\vec{R}_n+\vec{r}_n)} \\ &\quad\times \mathrm{Im}\, G^{+}(\vec{R}_n+\vec{r}_n,\vec{R}_n+\vec{r}',E) \\ &\quad\times U_{\vec{p}'m_s'} e^{i\vec{p}'\cdot(\vec{R}_n+\vec{r}')}. \end{aligned} \tag{13}$$

If the translational invariance property of the Green's function is taken into account and the Bloch theorem is applied for $\Phi_{\vec{p}m_s}$, one gets

$$\begin{aligned} G_{m_s m_s'}(\vec{p},\vec{p}',E) &= \frac{1}{\Omega}\int d^3r_n \int d^3r' U^{\times}_{\vec{p}m_s} e^{-i\vec{p}\cdot\vec{r}_n} \\ &\quad\times \mathrm{Im}\, G^{+}(\vec{r}_n,\vec{r}',E) U_{\vec{p}'m_s'} e^{i\vec{p}'\cdot\vec{r}'}\frac{1}{N}\sum_n e^{i(-\vec{p}+\vec{p}')\cdot\vec{R}_n} \\ &= \frac{1}{\Omega}\int d^3r_n \int d^3r' U^{\times}_{\vec{p}m_s} e^{-i\vec{p}\cdot\vec{r}_n} \\ &\quad\times \mathrm{Im}\, G^{+}(\vec{r}_n,\vec{r}',E) U_{\vec{p}'m_s'} e^{i\vec{p}'\cdot\vec{r}'}\Delta(-\vec{p}+\vec{p}'), \end{aligned} \tag{14}$$

leading to the following property:

$$G_{m_s m_s'}(\vec{p},\vec{p}',E) = G_{m_s}(\vec{p},\vec{p}',E)\delta_{m_s m_s'}\Delta(-\vec{p}'+\vec{p}). \tag{15}$$

With the Green's function in the coordinate representation as given by Eq. (1), Eq. (14) leads to

$$\begin{aligned} G_{m_s}(\vec{p},\vec{p},E) &= \frac{1}{\Omega}\int d^3r_{0q}\int d^3r'_{0q} U^{\times}_{\vec{p}m_s} e^{-i\vec{p}\cdot(\vec{r}_{0q}+\vec{R}_q)} \\ &\quad\times \mathrm{Im}\left[\sum_q\sum_{\Lambda\Lambda'} Z_{\Lambda}^{q}(\vec{r}_{0q},E)\tau^{0q0q}_{\Lambda\Lambda'}(E) Z_{\Lambda'}^{q\times}(\vec{r}'_{0q},E)\right. \\ &\quad - \sum_{\Lambda} Z_{\Lambda}^{q}(\vec{r}_{0q},E) J_{\Lambda}^{q\times}(\vec{r}'_{0q},E)\,\theta(\vec{r}'_{0q}-\vec{r}_{0q}) \\ &\quad \left. + J_{\Lambda}^{q\times}(\vec{r}_{0q},E) Z_{\Lambda}^{q}(\vec{r}'_{0q},E)\,\theta(\vec{r}_{0q}-\vec{r}'_{0q})\right] \\ &\quad\times U_{\vec{p}m_s} e^{i\vec{p}\cdot(\vec{r}'_{0q}+\vec{R}_q)} \\ &\quad + \frac{1}{\Omega}\sum_q{\sum_{n'q'}}'\int d^3r_{0q}\int d^3r'_{n'q'} U^{\times}_{\vec{p}m_s} e^{-i\vec{p}\cdot(\vec{r}_{0q}+\vec{R}_q)} \\ &\quad\times \mathrm{Im}\left[\sum_{\Lambda\Lambda'} Z_{\Lambda}^{nq}(\vec{r}_{0q},E)\tau^{nqn'q'}_{\Lambda\Lambda'}(E) Z_{\Lambda'}^{n'q'\times}(\vec{r}'_{n'q'},E)\right] \\ &\quad\times U_{\vec{p}m_s} e^{i\vec{p}'\cdot(\vec{r}'_{n'q'}+\vec{R}_{n'}+\vec{R}_{q'})}. \end{aligned} \tag{16}$$

The scattering path operators for the site-diagonal part is τ^{0q0q} and $\tau^{nqn'q'}$ for the non-site-diagonal part, where $q(q')$ numbers the sites within the unit cell $n(n')$. Finally, the following expression for the momentum representation Green's function to be inserted into Eq. (6) is obtained:

$$\begin{aligned} G_{m_s}(\vec{p},\vec{p},E) &= \frac{1}{\Omega}\,\mathrm{Im}\sum_q\left[\sum_{\Lambda\Lambda'} M^{q}_{m_s\Lambda} t^{q}_{\Lambda\Lambda'} M^{q*}_{m_s\Lambda'} - \sum_{\Lambda}\tilde{M}^{q}_{m_s\Lambda m_s}\right] \\ &\quad + \frac{1}{\Omega}\,\mathrm{Im}\sum_q\sum_{\Lambda\Lambda'} M^{q}_{m_s\Lambda}[\tau^{qq}(\vec{p})-t^{q}]_{\Lambda\Lambda'} M^{q*}_{m_s\Lambda'} \\ &\quad + \frac{1}{\Omega}\,\mathrm{Im}\sum_q\sum_{q'\neq q} e^{-i\vec{p}\cdot(\vec{R}_q-\vec{R}_{q'})} \\ &\quad\times\sum_{\Lambda\Lambda'} M^{q}_{m_s\Lambda}\tau^{qq'}_{\Lambda\Lambda'}(\vec{p}) M^{q'*}_{m_s\Lambda'}. \end{aligned} \tag{17}$$

The quantities $M^{q}_{m_s\Lambda}$ and $M^{q}_{m_s\Lambda m_s'}$ are the overlap matrix elements of the regular and irregular solutions of the Dirac equation and the eigenfunctions of the momentum operator:

$$M^{q}_{m_s\Lambda} = M^{q}_{m_s\Lambda}(\vec{p},E) = \langle\Phi_{\vec{p}m_s}|Z^{q}_{\Lambda}\rangle \tag{18}$$

and

$$\begin{aligned} \tilde{M}^{q}_{m_s\Lambda'' m_s'} &= M^{q}_{m_s\Lambda'' m_s'}(\vec{p},E) \\ &= \langle\Phi_{\vec{p}m_s}(\vec{r})|[Z^{q}_{\Lambda''}(\vec{r}) \\ &\quad\times J^{q\times}_{\Lambda''}(\vec{r}')\Theta(r'-r)J^{q}_{\Lambda''}(\vec{r})Z^{q\times}_{\Lambda''}(\vec{r}')\Theta(r-r')] \\ &\quad\times|\Phi_{\vec{p}m_s'}(\vec{r}')\rangle. \end{aligned} \tag{19}$$

The first term in Eq. (17) is the single-site part, with the

TABLE I. Magnetic moments of U and Fe (in μ_B) in UFe_2. The SPR-KKR calculated magnetic moments are compared with the LMTO results of Eriksson *et al.* (Ref. 2) and Antonov *et al.* (Ref. 21) and with experimental data determined by neutron scattering (Ref. 4), XMCD (Ref. 6), and magnetic Compton scattering (Ref. 8) investigations.

	U			Fe			Total		
	m_{spin}	m_{orb}	m_{tot}	m_{spin}	m_{orb}	m_{tot}	m_{spin}	m_{orb}	m_{tot}
LMTO, LSDA[a]	−0.71	0.47	−0.24	0.75	0.07	0.82	0.79	0.61	1.40
LMTO, LSDA+OP[a]	−1.03	0.88	−0.15	0.82	0.07	0.89	0.61	1.02	1.63
LMTO, LSDA[b]	−0.61	0.35	−0.26	0.68	0.06	0.74	0.75	0.47	1.22
LMTO, LSDA+U(OP)[b]	−0.71	0.72	0.01	0.71	0.08	0.79	0.71	0.88	1.59
LMTO, LSDA+U[b]	−1.83	3.08	1.25	1.14	0.20	1.34	0.45	3.48	3.93
KKR, LSDA*	−0.56	0.29	−0.27	0.69	0.06	0.75	0.82	0.41	1.23
Expt.[c]	−0.22	0.23	0.01	0.59	—	—	—	—	1.19
Expt.[d]	−0.20	0.21	0.01	—	—	—	—	—	—
Expt.[e]	−0.20	—	—	0.52	—	—	—	—	—

[a]Reference 2.
[b]Reference 21.
[c]Reference 4.
[d]Reference 6.
[e]Reference 8.

single-site t matrix t^q describing the scattering from the atom sitting on site q. For the energy integration of this term, a path along the real axis will be used. This way, the matrices $\tilde{M}^q_{m_s\Lambda m_s'}$ do not have to be evaluated, because they contain the irregular solutions of the Dirac equations which contribute to Eq. (17) only for complex energies. This applies because only the imaginary part has to be considered at the end.

The second term is the so-called backscattering term that can be evaluated through an energy integration in the complex plane, along an arclike contour path with only few energy mesh points. In the last term of Eq. (17) the sum over the cell index n' has been performed:

$$\tau^{qq'}(\vec{p}) = \sum_{n'} e^{i\vec{p}\cdot\vec{R}_n}\tau^{nqn'q'}. \tag{20}$$

While the first two terms in Eq. (17) give the contributions to the momentum representation Green's function of the various sites q within a unit cell, the last term represents interference terms of all site combinations $q-q'$ with $q \neq q'$.

III. RESULTS AND DISCUSSIONS

A. Magnetic moments

The spin and orbital magnetic moments of U and Fe in UFe_2 resulting from our fully relativistic KKR calculation are given in Table I.

These results are compared with the experimental data stemming from neutron scattering,[4] XMCD,[6] and magnetic Compton scattering[8] investigations and with results of LMTO calculations.[2,21] The U^{5f} and Fe^{3d} magnetic moments of the present KKR calculations and LMTO (Ref. 2) calculations are presented in addition in Table II. The theoretical KKR-based values for the spin and orbital moments compare rather well with the corresponding recent LSDA-based fully relativistic LMTO calculations of Antonov *et al.*[21]

In addition to LSDA-based results Table I gives results[2,21] that have been obtained by including the so-called orbital polarization (OP) correction term.[2] This correction primarily influences the orbital magnetic moment and for that reason should influence the MCP only slightly. For the sake of completeness results obtained on the basis of the LSDA+U scheme[21] have been added well. As one notes, the treatment of correlation effects by including a corresponding correction to the LSDA-based Hamiltonian strongly influences spin as well as orbital magnetic moments.

B. Magnetic Compton profile

The magnetic Compton profile (MCP) of UFe_2 has been calculated using the fully relativistic KKR method and the formalism described in Sec. II B. To reveal the influence of the spin-orbit coupling on the magnetic Compton profile of UFe_2 these calculations have been done in addition with the spin-orbit coupling suppressed. The comparison of corre-

TABLE II. Magnetic moments of U^{5f} and Fe^{3d} (in μ_B) in UFe_2. The SPR-KKR calculated magnetic moments are compared with the corresponding LMTO results of Eriksson *et al.* (Ref. 2) obtained without and with the orbital polarization (OP) correction term.

	U^{5f}		Fe^{3d}	
	m_{spin}	m_{orb}	m_{spin}	m_{orb}
KKR, LSDA	−0.45	0.27	0.70	0.06
LMTO, LSDA	−0.58	—	0.73	—
LMTO, LSDA-OP	−0.83	0.88	—	—

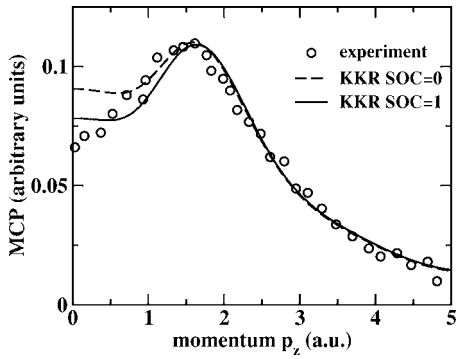

FIG. 1. Theoretical magnetic Compton profile of UFe_2 with the spin-orbit coupling included (SOC=1) and suppressed (SOC=0). The spectra have been convoluted with a Gaussian of a full width at half maximum (FWHM) 0.78 a.u. in line with the corresponding experimental data of Lawson *et al.* (Ref. 8).

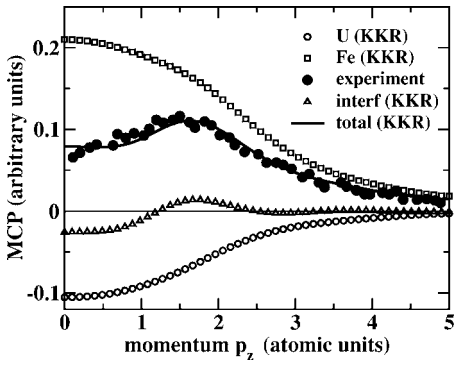

FIG. 2. The magnetic Compton profile of UFe_2 (solid line) decomposed into U (open circles), Fe (open squares), and interference term (U-Fe) (open triangles) contributions. The profiles have been broadened with a Gaussian of FWHM=0.78 a.u., according to the experimental momentum resolution. The experimental data of Lawson *et al.* (Ref. 8) are represented by circles.

sponding results is presented in Fig. 1 together with experimental data.[8] The theoretical KKR calculations have been convoluted with a Gaussian of 0.78 a.u. width according to the reported experimental resolution.

As can be seen, in the high-momentum region ($p_z \geqslant 2$ a.u.) the spin-orbit coupling does not influence the magnetic spin density. This does not apply for the low-momentum region ($p_z \leqslant 2$ a.u.), where the calculation with spin-orbit switched off lies well above the experimental magnetic Compton profile. On the other hand, the strong dip in the experimental profile in the low-momentum region is nearly perfectly reproduced by the fully relativistic calculations. Altogether these lead to a theoretical profile that is in very satisfying agreement with experiment.

C. Decomposition of the magnetic Compton profile of UFe_2

For a detailed discussion and interpretation of the MCP of UFe_2 it is necessary to decompose it into its site-projected contributions. This can be done on the basis of the representation of the MCP in terms of the Green's function as given by Eq. (17).

As is obvious from the third term in Eq. (17), besides the strictly site-projected contributions there is a site-site (q-q') interference term. The results of a corresponding decomposition are presented in Fig. 2. As can be seen, Fe gives a dominating (positive) contribution, with its variation with momentum p_z reflecting the relatively localized spin magnetic moment due to the d electrons. The negative sign of the U contribution, on the other hand, reflects the antiparallel orientation of the U spin moment with respect to the Fe spin moment. In line with the component resolved spin moments listed in Tables I and II, the U contribution to the MCP compensates to a large extent for that of Fe. However, the ratio of the integrals over the partial Fe and U MCP's found to be -2.66 is quite different from the ratio of the corresponding spin moments, $\mu_{spin}^{Fe}/\mu_{spin}^{U}=-1.93$. This implies that in general there is no strict one-to-one correspondence between the integrals over the component-projected MCP's and the corresponding spin magnetic moments. This has to be ascribed to the influence of the matrix elements given in Eqs. (18) and (19) and the interference term that occurs in addition to the site-projected contributions to the MCP [third term on the right-hand side of Eq. (17)]. As Fig. 2 shows, the interference contribution is much smaller in amplitude than the other two. Nevertheless, neglect of the interference term is by no means justified. In particular it is obviously responsible for the dip in the low-momentum regime, as the interference term is negative for $p_z \leqslant 1.2$ a.u. and positive for $p_z \geqslant 1.2$ a.u. Here it should be noted that a similar decomposition of the magnetic Compton profile has been made by Srajer *et al.*[13] for the Invar alloy Fe_3Pt. In this case a rather small Fe-Pt interference contribution was found. Presumably this has to be ascribed to the fact that the Fe moment by far dominates in the case of Fe_3Pt, while the small spin moment is induced only by the neighboring Fe atoms. In contrast to this the spin magnetic moments of Fe and U in UFe_2 are comparable in magnitude (see above).

The decomposition of the theoretical MCP shown in Fig. 2 can be compared directly to the decomposition of the experimental MCP suggested by Lawson *et al.*[8] These authors fitted the experimental profile using partial Compton profiles for Fe $3d$ and U $5f$, which were deduced from atomic calculations. In addition there is a diffuse component, labeled *spd*, which is modeled as the sum of a U $6d$ free-atom-like profile and a free-electron parabola smeared with the experimental resolution function. The weights of these three empirical contributions have been determined by fitting the total experimental MCP, which is reproduced in a rather satisfying way by this procedure. Figure 3 shows the resulting individual contributions obtained from the fit together with the corresponding contributions of the theoretical MCP obtained within the present work (see Fig. 2).

Obviously, the contribution of the Fe site obtained from the KKR calculations agrees fairly well with the fitted contribution based on the atomiclike profile of the Fe $3d$ states. For the U site, on the other hand, the partial profile based on the atomiclike U $5f$ states is much more spread out along the p_z axis, indicating a stronger localization in real space than found by our KKR calculations. More important, however, seems to be the fact that the fitting procedure leads to a

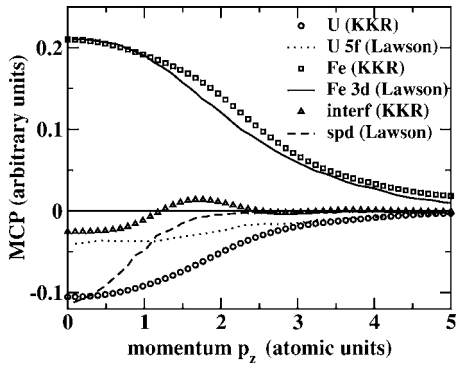

FIG. 3. The partial contributions to the magnetic Compton profile of UFe_2: U (circles), Fe (squares), and interference (triangles) terms resulting from the SPR-KKR calculation, together with the "Fe 3*d*" (solid line), "U 5*f*" (dotted line), and "*spd*" (dashed line) terms used by Lawson *et al.* (Ref. 8) to fit the experimental data.

contribution of the U site to the MCP that is too small. This is compensated in the fit by the diffuse term that is too large in amplitude in the low-momentum regime. According to our direct calculation of the partial contributions, there is no reason for a possible representation of the interference term as a sum of U 6*d* free-atom profile and a free-electron parabola. Our KKR band-structure calculations give a spin moment on *s*, *p*, and *d* orbitals of U that is about $\simeq 20\%$ of the U *f* spin moment (see Tables I and II). So there is no evidence for such a big negative diffuse contribution compared with the U 5*f* one as suggested by Lawson *et al.*[8]

IV. CONCLUSIONS

The spin and orbital magnetic moments and the magnetic Compton profile of UFe_2 system have been determined using the spin-polarized relativistic Korringa-Kohn-Rostoker band-structure method. The influence of the spin-orbit coupling on the MCP of UFe_2 along the [001] direction has been demonstrated. The MCP spectra have been decomposed into U, Fe, and interference terms in order to compare the individual contributions and to allow for a detailed discussion.

Our results for UFe_2 demonstrate that due to an appreciable site-site interference contribution, an unambigous decomposition of the MCP into site or component, respectively, contributions is in general not possible. In addition it turned out that the integrals over the component-projected contributions to the MCP do not strictly scale with the corresponding spin magnetic moment due to the influence of the overlap matrix elements involved.

[1] M. S. S. Brooks and P. J. Kelly, Phys. Rev. Lett. **51**, 1708 (1983).
[2] O. Eriksson, M. S. S. Brooks, and B. Johansson, Phys. Rev. B **41**, R7311 (1990).
[3] M. Wulff, G. H. Lander, B. Lebech, and A. Delapalme, Phys. Rev. B **39**, 4719 (1989).
[4] M. Wulff, G. H. Lander, A. Delapalme, B. Lebech, and J. C. Spirlet, Physica B **156-157**, 836 (1989).
[5] B. Lebech, M. Wulff, G. H. Lander, J. Rebizant, J. C. Spirlet, and A. Delapalme, J. Phys.: Condens. Matter **1**, 10229 (1989).
[6] M. Finazzi, Ph. Sainctavit, A. M. Dias, J. P. Kappler, G. Krill, J. P. Sanchez, P. Dalmas de Réotier, A. Yaouanc, A. Rogalev, and J. Goulon, Phys. Rev. B **55**, 3010 (1997).
[7] M. S. S. Brooks, O. Eriksson, B. Johansson, J. J. M. Franse, and P. H. Frings, J. Phys. F: Met. Phys. **18**, L33 (1988).
[8] P. K. Lawson, M. J. Cooper, M. A. G. Dixon, D. N. Timms, E. Zukowski, F. Itoh, and H. Sakurai, Phys. Rev. B **56**, 3239 (1997).
[9] P. E. Mijnarends and A. Bansil, Phys. Rev. B **13**, 2381 (1976).
[10] B. L. Gyorffy and G. M. Stocks, J. Phys. F: Met. Phys. **10**, L321 (1980).
[11] Y. Kubo and S. Asano, Phys. Rev. B **42**, 4431 (1990).
[12] D. L. Anastassopoulos, G. D. Priftis, N. I. Papanicolaou, N. C. Bacalis, and D. A. Papaconstantopoulos, J. Phys.: Condens. Matter **3**, 1099 (1991).
[13] G. Srajer, C. J. Yahnke, D. R. Haeffner, D. M. Mills, L. Assoufid, B. N. Harmon, and Z. Zuo, J. Phys.: Condens. Matter **11**, L253 (1999).
[14] P. Weinberger, *Electron Scattering Theory for Ordered and Disordered Matter* (Oxford University Press, Oxford, 1990).
[15] H. Ebert, in *Electronic Structure and Physical Properties of Solids*, editted by H. Dressé (Springer, Berlin, 2000), Vol. 535, p. 191.
[16] M. E. Rose, *Relativistic Electron Theory* (Wiley, New York, 1961).
[17] H. Ebert *et al.*, The Munich SPR-KKR package, version 2.1.1, 2002, http://olymp.cup.uni-muenchen.de/ak/ebert/SPRKKR.
[18] S. H. Vosko, L. Wilk, and M. Nusair, Can. J. Phys. **58**, 1200 (1980).
[19] S. W. Lovesey and S. P. Collins, *X-Ray Scattering and Absorption by Magnetic Materials* (Clarendon Press, Oxford, 1996), Chap. 7.
[20] M. A. G. Dixon, J. A. Duffy, S. Gardelis, J. E. McCarthy, M. J. Cooper, S. B. Dugdale, T. Jarlborg, and D. N. Timms, J. Phys.: Condens. Matter **10**, 2759 (1998).
[21] V. N. Antonov, B. N. Harmon, and A. N. Yaresko, Phys. Rev. B **68**, 214424 (2003).